This manuscript was accepted by J. Chem. Phys. Click here to see the version of record.

CO adsorption on nanoislands: Ni on Au(111)

Joshua I. Cohen and R. G. Tobin[1)]

Department of Physics and Astronomy, Tufts University, Medford, Massachusetts, 02155, USA

The adsorption behavior of CO on Ni islands grown on Au(111) was studied with a combination of TPD, FTIR and surface resistivity measurements. The Au(111) herringbone reconstruction provides a template for the growth of ordered Ni islands, with evidence for the presence of strain and Au atoms within the islands. The islands grow radially until $\theta_{Ni} \approx 0.3\ ML$, after which subsequent Ni atoms contribute primarily to a second layer. We study saturated CO adsorption at 227 K over a range of Ni island sizes, and find layer-dependent adsorption properties. For single-layer islands at low Ni coverage, CO adsorbs primarily in the atop position and desorbs at lower temperatures than on pure Ni, with a saturation CO coverage of about 0.5 CO/Ni. As second layer Ni grows, saturated CO coverages on the Ni approach unity, with higher desorption temperatures, but still with primarily atop CO. Based on previous studies, we propose that in the first Ni layer, ligand effects from the Au substrate and possibly Au in the islands and strain due to the Ni/Au lattice mismatch affect the Ni-CO bonds. CO adsorption behavior on the two-layer islands is qualitatively explained by a decrease in Au nearest neighbors and the presence of a more expanded/corrugated structure.

[1] Author to whom correspondence should be addressed. Electronic mail: roger.tobin@tufts.edu

This manuscript was accepted by J. Chem. Phys. Click here to see the version of record.

I. INTRODUCTION

The surface chemistry of nanoparticles and bimetallic systems can differ greatly from that of close-packed, pure, extended surfaces.[1-16] These systems display tunable properties, and are of great interest not only from a fundamental science perspective, but also from a practical viewpoint, with potential applications in fields such as medicine, telecommunications, and environmental remediation.[1] These unique chemical properties are often understood as being due to three different effects: ensemble, ligand, and strain. The ensemble effect is due to a particular geometric orientation of atoms,[15, 17] the ligand effect to heterometallic bonding that changes the electronic environment,[18, 19] and strain effects to lattice constant differences and variations in coordination number.[17, 20] These effects are related to the width and position of the *d*-band relative to the Fermi level, and can be cumulative, yet difficult to separate.[18] In this paper we study the effects of nanoparticle size, structure, and composition on the adsorption properties of CO to Ni islands grown on Au(111), using temperature programmed desorption (TPD), Fourier transform infrared spectroscopy (FTIR), and surface resistivity measurements.

The Ni island on Au(111) system has been of interest in a variety of studies.[13, 21-26] When cleaned and annealed, the Au(111) surface configures into the herringbone reconstruction,[27-29] shown schematically in Figure 1(a), and described in more detail in Ref. 26. Chambliss et al. used scanning tunneling microscopy (STM) to study the behavior of Ni deposited onto herringbone-reconstructed Au(111), and found for low Ni coverages, Ni grew in an ordered array of single-layer nanometer-scale Ni islands.[27, 28] Second-layer growth begins before completion of the first layer, at a Ni coverage of approximately 0.3 ML.[25, 28] Figures 1(b) – 1(e) show schematically how the islands grow at the elbows of the reconstruction with increasing Ni coverage. Subsequent STM studies have refined this picture. Hannemann et al. found the islands

This manuscript was accepted by J. Chem. Phys. Click here to see the version of record.

possess considerable structure, and propose it is due to the large lattice mismatch of ~ 14% between Ni and Au.[22] Cullen et al. also observed structure within the islands deposited at room temperature (RT), and suggested the structure is due to intermixing of Ni and Au atoms, with intermixing increasing as deposition and annealing temperatures rise above 400 K.[30]

Previously, we studied surface resistivity ρ_s, changes to the Au(111) substrate due to the growth of the Ni islands.[26] Adsorbate-induced surface resistivity is known to be a first-layer effect,[31-34] and therefore can serve as an indirect probe of surface morphology. In our study of Ni islands, we found ρ_s to increase linearly with the Ni coverage θ_{Ni}, until a transition coverage, above which additional Ni atoms contributed very little to surface resistivity.[26] The transition point where ρ_s plateaued corresponded closely with the transition point (approximately 0.3 ML) where second layer Ni begins forming, according to STM studies. We concluded that Ni atoms in the first layer contribute evenly to ρ_s, while second layer Ni makes little to no contribution to ρ_s.[26]

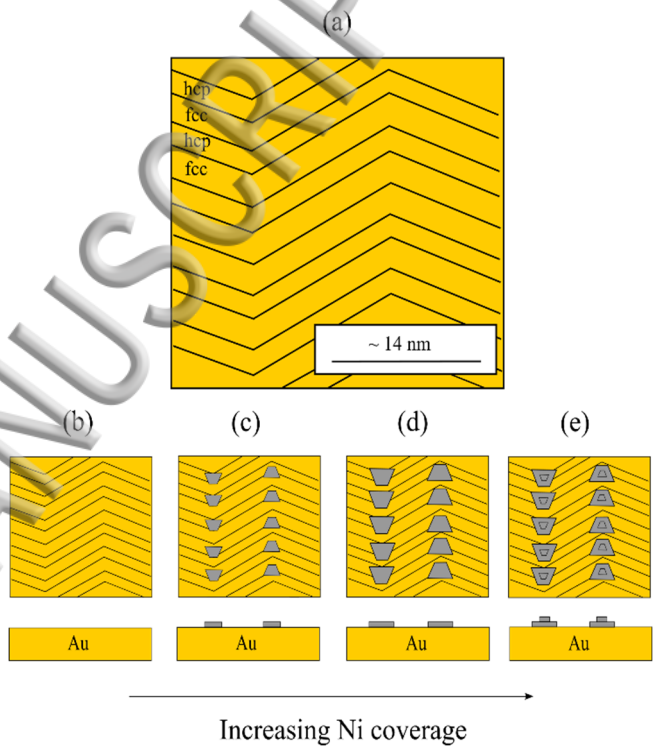

Figure 1: Schematic representation of Ni island growth on Au(111) based on STM images in Ref. 25 and 30 and growth details from Ref. 28. The islands preferentially nucleate at the elbows of the herringbone reconstruction. (a-b) clean Au(111) surface and the herringbone reconstruction. (c) small islands beginning to form at the elbows of the reconstruction. (d) as more Ni is deposited on the surface the islands grow outwardly. (e) at a certain coverage the islands form a second layer before filling in the first layer. Reproduced from J. Cohen and R.G. Tobin, J. Chem. Phys. **146**, 144703 (2017), with the permission of AIP Publishing.

This manuscript was accepted by J. Chem. Phys. Click here to see the version of record.

In the present experiment we also monitored surface resistivity during Ni deposition and during CO exposure as a probe of adsorption behavior. Previous studies of CO on pure Ni measured an increase in ρ_s.[35, 36] Our measurements of ρ_s due to Ni deposition were consistent with previous results.[26] No change in ρ_s was observed due to CO adsorption.

An additional way to investigate surface morphology and surface chemistry is by adsorption of a probe molecule. CO adsorption has been broadly studied on extended surfaces.[37-55] In studies of pure Au, CO has been shown to desorb by 190 K, below our experimental temperatures, and with an IR band around 2110 cm^{-1}, which is not observed in our work.[49-53] For this and other reasons detailed below, we do not expect CO bonding to the Au surface under our experimental conditions and assume that CO bonds only to the Ni islands. In the case of single crystal Ni, CO tends to bind in bridge and atop positions with IR peaks measuring between $1850 - 1924\ cm^{-1}$ and $2016 - 2076\ cm^{-1}$ respectively,[37, 38] with a maximum saturation coverage measured by Lauterbach et al. on Ni(100) of $\theta_{sat\ CO}^{Ni(100)} = 0.67 \pm 0.03\ ML$.[37] For atop and bridge CO, the CO molecular axis is normal to the surface, with the carbon atom bonding to one or two metal atoms respectively.[40, 56] We use a Ni(100) single crystal to compare and calibrate our TPD and FTIR data.

CO adsorption to other Ni-Au systems has also been studied experimentally and theoretically.[10-13, 19, 57, 58] At the temperatures relevant to our experiments, CO does not bind to Au,[10, 11] and in some cases has been shown to desorb fully from Au by 100 K.[13] TPD and FTIR studies of CO adsorption to Ni-Au alloy surfaces have found that the presence of Au decreases peak CO desorption temperatures from Ni by up to 100 K,[11] and leads to preferential atop site occupation of CO on Ni.[10] The decrease in peak desorption temperature has been investigated theoretically by DFT studies, which found the Ni-CO bond strength decreases as the number of

This manuscript was accepted by J. Chem. Phys. Click here to see the version of record.

Ni's Au nearest neighbors increases.[19, 57, 58] Huang et al.'s DFT study of CO adsorption on Ni/Au surface alloys showed that the weakening effect of Au on Ni-CO bonds is largest for bridge bonded CO,[19] which may contribute to the preferential occupation of atop sites.

We report experiments on the behavior of saturation CO adsorption as a function of Ni coverage on the Au surface. At Ni coverages where second layer Ni begins growing on top of the single-layer islands, significantly more CO adsorbs to the surface than expected, approaching a density of one CO per surface Ni atom at high Ni coverage. We measure CO only in the atop position with FTIR, and at low Ni coverages find TPD peak temperatures $\sim 100\ K$ lower than for CO on pure Ni, with asymmetrical broadening towards higher temperatures as Ni coverage increases. We interpret these observations in the context of ligand and strain effects seen in similar systems.

II. EXPERIMENTS

The substrates were commercial 150 nm thick × 1 cm × 1 cm epitaxial Au(111) films on mica.[59] Contact pads (50 nm Ag on top of 10 nm Cr) were deposited *ex situ* under high vacuum on the corners for electrical contacts and in the middle of one edge for thermocouple attachment. The sample was then attached to a custom sample mount described elsewhere.[60] Wires were connected to the contact pads using colloidal silver paint to enable resistivity and temperature measurements.[61] Details of the resistivity measurement can be found elsewhere.[26] The sample was transferred into an ultrahigh vacuum chamber (UHV, base pressure 7×10^{-11} Torr), where the remainder of processing and measurement was completed. The sample was cleaned by Ar^+ sputtering ($1\ keV, \sim 7\ \mu A/cm^2$) and then annealed at 573-600 K for 2 min. We found higher annealing temperatures damaged the sensitive electrical contacts. The sputtering/annealing process was repeated until no contaminants were detectable with Auger electron spectroscopy

This manuscript was accepted by J. Chem. Phys. Click here to see the version of record.

(AES). By comparing the background noise to the C signal, the maximum contaminant coverage is estimated to be 0.01 ML.

The herringbone reconstruction, which is essential to the growth of Ni nano-islands, is well established to be the equilibrium state of the clean Au(111) surface.[30, 62] Following annealing, submonolayer Ni was deposited by thermal evaporation from 99.99% purity Ni wire wrapped around a well-outgassed tungsten filament. The sample temperature was regulated at $296.1 \pm 0.1\ K$. Under these experimental conditions, an ordered array of Ni nanoislands is known to form over a considerable range of substrate temperatures, substrate preparation protocols, and deposition rates.[13, 21, 24, 25, 27, 28, 30] During deposition, the resistance of the Au film was continuously monitored. We are not able to directly determine the presence, size, or structure of the Ni nanoislands. Our previous work, however, showed measurements of surface resistivity, coupled with reported STM measurements, provide strong indirect evidence that the ordered array of Ni islands was present.[26] A central discovery in that work is that second layer Ni atoms make little to no contribution to surface resistivity, and our data in this experiment are consistent with primarily second layer growth in that coverage range.[26]

Following the formation of the Ni nanoislands, the sample was cooled to $227 \pm 0.1\ K$. This temperature was selected based on Lauterbach et al.'s work that showed Ni(100) is completely saturated by CO at this temperature.[37] Ni deposition was done at room temperature because island formation and Ni-Au concentrations within the islands appear to have some temperature dependence.[13, 30] We assume the islands did not change in composition or structure upon cooling. Background FTIR spectra were then collected (Mattson Cygnus 100, HgCdTe detector, unpolarized, $16\ cm^{-1}$ resolution). The sample was then exposed to 5L of CO ($1L = 1 \times 10^{-6}\ Torr \cdot s$) by backfilling the chamber while simultaneously measuring surface

This manuscript was accepted by J. Chem. Phys. Click here to see the version of record.

resistivity. Sample FTIR scans were then acquired with the same settings as the background spectrum. Following FTIR, TPD curves were collected with the sample in front of the residual gas analyzer (RGA) with a heating rate of $3-4\ K/s$. FTIR data was analyzed by simultaneously fitting a quadratic background and Gaussian function to the data. Analysis of TPD data will be discussed later.

Our measure of Ni coverage is based on a normalized ratio of Ni and Au Auger signals,

$$\xi = \frac{\frac{\sigma_{Au}}{\sigma_{Ni}}[Ni]/[Au]}{1+\frac{\sigma_{Au}}{\sigma_{Ni}}[Ni]/[Au]} \quad , \tag{1}$$

where $[Ni]$ is the 848 eV peak-peak height and $[Au]$ is the 239 eV peak-peak height. The ratio of Auger cross sections for pure Au and pure Ni, $\frac{\sigma_{Au}}{\sigma_{Ni}}$, is determined from the ratio $[Au]/[Ni]$ measured in our system for pure Au and pure Ni taken under identical conditions.

In the simplest approximation that the Auger signal comes exclusively from the topmost atomic layer and that Ni forms a single layer on Au, the Ni coverage θ_{Ni}, is simply equal to the Auger ratio ξ. For low Ni coverages, this assumption is supported by STM observations that found ξ and θ_{Ni} to agree.[25, 28] At higher coverages, it can be important to include the finite inelastic mean free path λ of the Auger electrons, which leads to contributions to the AES signal from buried layers.[26] In general, for higher Ni coverages, ξ tends to underestimate the total Ni coverage, but may overestimate the amount of exposed Ni on the surface, which is more relevant to adsorption. These effects would not affect our major conclusions.

While we do not directly image the surface to verify the island structure, there are strong reasons to assume that it is present. First, our previous resistivity study, along with reports of STM measurements, show the formation of Ni islands to be a robust process that is largely independent

This manuscript was accepted by J. Chem. Phys. Click here to see the version of record.

of experimental details.[13, 21, 24, 25, 27, 28, 30] We also monitored surface resistivity during Ni deposition for most of the runs in this study and again found a rolloff in resistivity above the Ni coverage at which second layer island growth is expected. Finally, as we show below, the CO adsorption behavior also shows a striking change at the same threshold Ni coverage.

At each Ni coverage, the saturation quantity of CO adsorbed to the Ni/Au(111) surface was determined by the area under the TPD curves, calibrated by comparison to measurements on Ni(100). Based on the measurements of Lauterbach et al. we take the saturation coverage of CO on Ni(100) to be 0.67 at 227 K.[37] Our measurements of CO uptake curves (CO coverage as a function of exposure) at two temperatures were consistent with that work, and also verified that exposures measured from ion gauge readings were consistent. The ratio of RGA signal to ion gauge reading during CO dosing, however, varied over time, possibly due to changes in electron multiplier sensitivity. To correct for these variations, the RGA signal for each TPD measurement was normalized using the ratio of RGA to ion gauge signals during the CO dose that immediately preceded it.

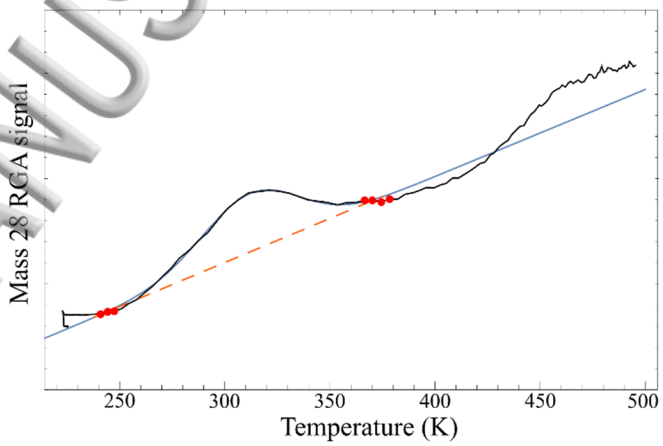

Figure 2: Background subtraction scheme for raw TPD data of CO on Ni/Au(111). Black curve is the raw TPD data. The red points are chosen to find the dashed line background curve that agrees closest with expectations of background behavior. The blue curve is the Gaussian fit plus the background curve. The behavior at $T > 450\ K$ is from the background and was observed even in experiments in which no Ni was deposited on the Au.

A typical, calibrated TPD signal for saturated CO on Ni islands on Au(111) is displayed in Figure 2. The behavior of the signal for T > 450 K was present in all experiments, including those with no Ni deposited on the Au surface, and is attributed to background desorption from other

pgts of the sample mount, but it was not reproducible enough for accurate subtraction. Instead, we found the most consistent background subtraction scheme was to fit a line to points before and after the peak that best isolated the characteristic CO desorption peak. This process is illustrated in Figure 2 by the discrete points before and after the peak, and the dashed line going through them. A Gaussian was fit to the background-subtracted data to determine peak area, width and maximum temperature T_{max}. The solid blue curve in Figure 2 represents the Gaussian plus the linear background. This background subtraction scheme is the largest source of uncertainty in our TPD data. We estimated uncertainty by varying the choice of points for fitting the linear background, resulting in background curves of varying slopes that still represent reasonable background behavior.

For experimental comparison, we collected FTIR (unpolarized, 8 cm^{-1} resolution) and TPD data for CO on a 2-mm thick × 3 cm × 1 cm Ni(100) single crystal using procedures as close as possible to those used for the Au samples. We cleaned the sample with Ar^+ sputtering and then annealed to 950 K for 10 minutes. Based on AES ratios, we estimate roughly 0.04 ML of C remained on the Ni surface. We also found additional Auger diffraction peaks reported for clean Ni(100),[63] suggesting a considerable fraction of the sample is clean Ni(100). We collected FTIR data at 200 K at CO saturation, and found bridge CO at 1956 cm^{-1} and atop CO at 2072 cm^{-1}, both with widths of about 35 cm^{-1}. Because TPD curve areas are expected to scale with sample area, our TPD analysis on the Ni(100) single crystal was done by covering the ends with Cu foil so that the exposed central area was comparable to the 1 × 1 cm Au(111) samples. Experiments were done above Cu-CO desorption temperatures.[32] We measured uptake curves at 226 K and 298 K, and found good agreement of our TPD and FTIR data with Lauterbach et al.'s data.[37] We found two TPD peaks at 298 K and 374 K, which are slightly different than Lauterbach et al. who found

This manuscript was accepted by J. Chem. Phys. Click here to see the version of record.

peaks at 280 K and 440 K. We attribute these differences to the small amount of C still present on our sample and the difference in heating rates.[64]

To estimate the CO coverage on the Ni/Au(111) sample, we compare our TPD areas to our saturated Ni(100) single crystal TPD area. We use the symbol $\vartheta_{CO}^{Ni/Au}$ to represent our approximation for the coverage of CO relative to the full exposed surface area of the sample, including both Au and Ni-covered regions. It is defined as follows:

$$\vartheta_{CO}^{Ni/Au} = \theta_{sat\ CO}^{Ni(100)} \frac{TPD_{sat}[Ni/Au]}{TPD_{sat}[Ni(100)]} \quad , \tag{2}$$

where $TPD_{sat}[x]$ is the TPD area under the curve of CO saturation on surface x.

III. RESULTS AND ANALYSIS

Figure 3 shows background-subtracted TPD scans for saturation coverages of CO adsorbed to the Ni islands on Au(111) for different Ni coverages. A small amount of CO was detected in experiments in which there was little or no Ni on the surface, $\xi < 0.01$ and $\xi = 0.1$. These TPD peaks are short and broad, consistent with desorption from other parts of the sample mount that heat at varying rates, resulting in very broad TPD signals. As the Ni coverage increases, and the island size grows, the saturation coverage increases, since there are more surface Ni atoms available. The curves for higher Ni coverage ξ take on a more defined shape, with the TPD peak temperature T_{max}, nearly

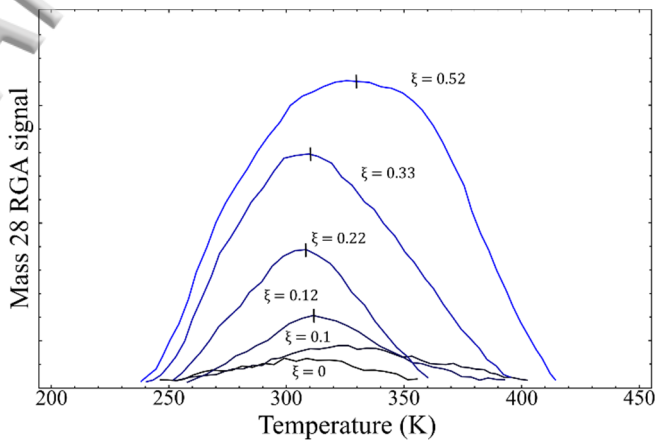

Figure 3: Background subtracted TPD signals from saturated coverages of CO on Ni/Au(111). Each curve represents a higher Ni coverage on Au(111) as measured by AES. The vertical lines indicate the peak temperature of the TPD signal.

This manuscript was accepted by J. Chem. Phys. Click here to see the version of record.

constant up to $\xi \approx 0.3$, but shifting upwards for higher ξ as the desorption peak broadens towards the high-temperature side. Since the evolution of the TPD curves at high Ni coverage is characterized more by a gradual broadening towards the high-temperature side, rather than by the growth of a distinct high-temperature feature, we interpret this evolution as the gradual emergence of a broad distribution of higher binding-energy bonding configurations. We cannot rule out, however, the possibility that the broad peak conceals two or more distinct but unresolved features.

Figure 4 shows the normalized integrated TPD area for saturation coverages of CO on Ni/Au(111), $\vartheta_{CO}^{Ni/Au}$, as a function of Ni coverage as measured by the AES ratio, ξ. Each data point in Figure 4 was collected after sputtering, annealing, and a fresh deposition of Ni onto the Au sample, and dosing with CO to saturation (5L). The peak area grows roughly linearly with ξ for low ξ, but then increases more rapidly for $\xi > 0.3$. By comparing slopes in the low and high ξ regions, we find that about 2-3 times as much CO adsorbs per increment in ξ in the higher coverage regime than at low Ni coverage.

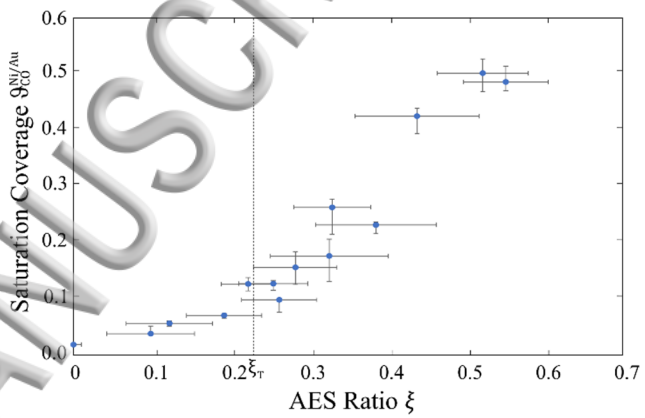

Figure 4: Saturation coverages of CO on Ni/Au(111) $\vartheta_{CO}^{Ni/Au}$, as a function of Ni coverage as measured by the AES ratio ξ. The dashed line shows ξ_T, where second layer Ni growth is expected to begin. $\vartheta_{CO}^{Ni/Au}$ grows linearly for low ξ, but transitions to higher saturation coverages for high ξ.

The increasing slope seen in Figure 4 is surprising considering the established growth model of this system.[24, 25, 27, 28, 30] At Ni coverages above about 0.3 ML, indicated by the dashed line at ξ_T in Fig. 4, additional Ni forms a second layer on top of the existing single-layer islands. Since each added second-layer Ni atom covers a first-layer atom, the number of exposed surface

This manuscript was accepted by J. Chem. Phys. Click here to see the version of record.

Ni atoms should stop increasing. Thus, if the saturation ratio of adsorbed CO to surface Ni remained fixed, we would expect the total amount of adsorbed CO to level off. This would manifest as a decrease in slope in Figure 4 in the region where second layer Ni is present, for $\xi > \xi_T$, since at this point additional Ni atoms added to the system are not expected to create new CO adsorption sites, except perhaps for a few edge sites. We instead see not only a continued increase in the total amount of adsorbed CO, but an *increase* in slope in that region, suggesting there is a substantially higher concentration of CO molecules per exposed Ni atom for second layer growth than during first layer growth.

We can rule out CO adsorption to the Au surface. First, our TPD and FTIR data are consistent with adsorption on Ni, with no additional peaks that would indicate Au-CO bonding. We also measured no change in surface resistivity during CO exposure, which would be expected for direct adsorption of CO on Au.[31-34] Studies of CO adsorption to pure Au and bimetallic Ni-Au systems do not find CO adsorption to Au at 227 K.[11, 13, 49, 51-53] The remainder of our analysis therefore assumes CO is adsorbing only to Ni atoms.

Our results, then, suggest that either the structure and growth of the Ni islands are more complicated than previously understood, or that CO adsorption on Ni nanoislands is substantially different from adsorption on crystals, with much higher local CO densities. To estimate the ratio of adsorbed

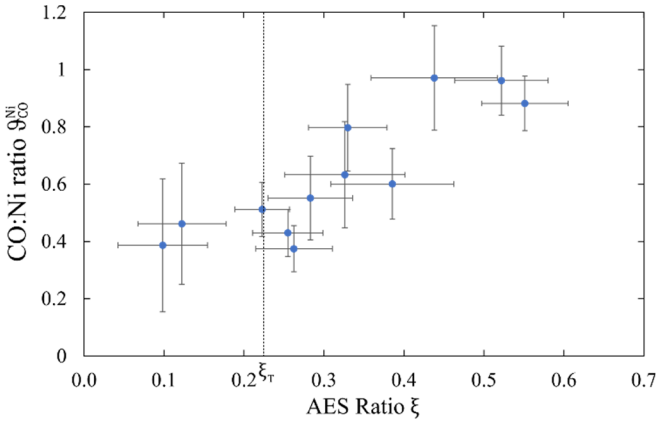

Figure 5: The estimated ratio of adsorbed CO to surface Ni atoms, ϑ_{CO}^{Ni}, plotted against Auger ratio ξ, our estimate for the percentage of the Au surface area covered by Ni.

This manuscript was accepted by J. Chem. Phys. Click here to see the version of record.

CO to surface-exposed Ni, ϑ_{CO}^{Ni}, we divide the overall CO surface concentration by our measure of surface Ni coverage, ξ:

$$\vartheta_{CO}^{Ni} = \frac{\vartheta_{CO}^{Ni/Au}}{\xi} \approx \frac{\#\ of\ CO\ molecules}{\#\ of\ Ni\ surface\ atoms} \quad (3)$$

Figure 5 plots ϑ_{CO}^{Ni} vs ξ, and for low ξ, ϑ_{CO}^{Ni} is roughly constant with an average ratio of 0.45 ± 0.14 CO/Ni, roughly consistent with saturation coverages on Ni single crystal surfaces. As ξ increases past ξ_T, where second layer Ni growth is expected to begin, ϑ_{CO}^{Ni} also increases and approaches an average ratio of 0.94 ± 0.13 CO/Ni, substantially higher than is typically found in single-crystal studies. The relatively large uncertainty in the absolute CO/Ni ratio is due largely to the relatively high uncertainty in the surface Ni coverage.

The CO adsorption enhancement seen in Figures 4 and 5 grants a new perspective on the growth, composition, structure and chemistry of these Ni nanoislands. The number of CO adsorption sites grows roughly linearly with Ni coverage for lower Ni coverage, but new CO adsorption sites seem to appear much more quickly than expected for higher Ni coverage, and the CO/Ni ratio is much higher than expected from single-crystal experiments. In Figure 3, as the Ni coverage increases beyond ξ_T, the high-temperature side of the TPD curves broadens out considerably, causing an upwards shift of the peak temperature T_{max}. Figure 6 plots T_{max} as a function of ξ, and shows a monotonic increase beginning near $\xi \approx 0.3$, the coverage at which second-layer Ni growth begins

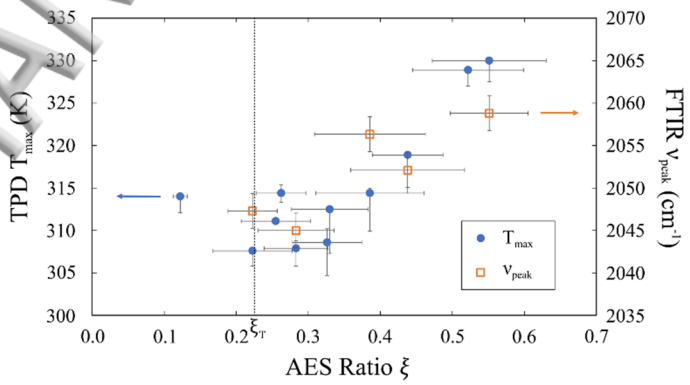

Figure 6: TPD T_{max} (left axis) and FTIR ν_{peak} (right axis) vs. ξ for CO on Ni/Au(111). Both quantities begin trending upwards as second layer Ni growth begins.

This manuscript was accepted by J. Chem. Phys. Click here to see the version of record.

and ϑ_{CO}^{Ni} begins to increase. This shift towards a higher T_{max} suggests the gradual emergence of a distribution of adsorption sites with higher binding energies. Step and kink adsorption sites have a higher binding energy than normal sites,[17, 65, 66] and it is possible the second Ni layer leads to a more complex morphology with varied binding environments.

Figure 7 shows FTIR spectra for saturated CO on Ni islands, with corresponding ξ values next to the curves, while the right axis in Figure 6 shows the IR peak frequencies ν_{peak}, plotted as a function of ξ. The peak frequency ν_{peak} centers around 2050 cm^{-1}, consistent with atop CO on Ni.[37, 38, 48] It is surprising that on these islands we only measure CO in the atop position with FTIR, while the corresponding T_{max} values from the TPD curves are 50 – 100 K lower than T_{max} values for saturated atop CO on pure Ni from both the literature[11, 37] and our measurements. Studies of adsorption on Ni-Au alloys have found the presence of Au affects the Ni-CO bond by reducing peak desorption temperatures and leading to preferential atop site occupation.[10, 11] It is possible, therefore, that CO's lower desorption temperature and preference for atop sites on Ni nanoislands is due to the number of Ni's Au nearest neighbors from either the Au substrate or intermixed Au in the islands. The upwards shift of peak

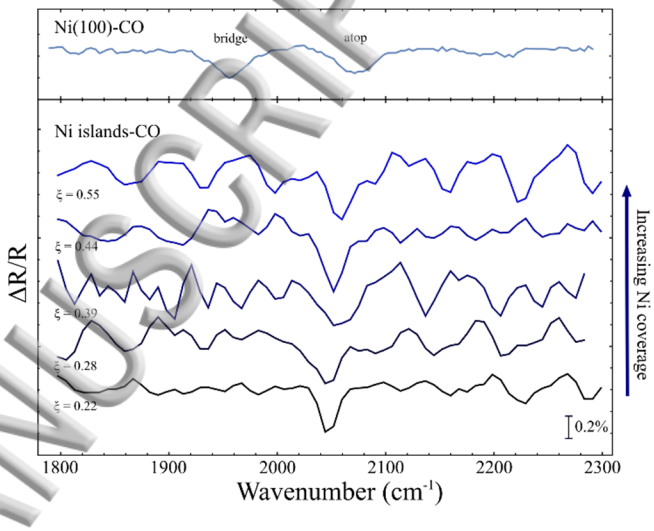

Figure 7: Top: FTIR spectrum after quadratic background subtraction of saturated CO on Ni(100) at 200 K with 8 cm^{-1} resolution. Bottom: FTIR spectra after quadratic background subtraction for saturated CO on Ni islands on Au(111) at 227 K with 16 cm^{-1} resolution. Ni coverage increases for higher curves. The higher signal-to-noise ratio in the single crystal data is due to the sample's larger surface area.

This manuscript was accepted by J. Chem. Phys. Click here to see the version of record.

desorption temperatures seen at higher Ni coverages could then be due to a decrease in the number of Au nearest neighbors during second layer growth.

The top of Figure 7 shows FTIR spectra for saturated CO adsorbed to single crystal Ni(100), and the bottom part shows saturated CO adsorbed to different size Ni islands on Au(111). For Ni(100), CO adsorbs in bridge and atop positions with similar intensities, while for the Ni islands, we only observe a peak due to atop CO. As the Ni islands increase in size, the integrated IR intensity remains nearly constant, and comparable to the total (bridge + atop) intensity for a saturation coverage of CO on Ni(100). IR intensity is affected by many factors, including site- and coverage-dependent polarizabilities, differences in substrate reflectance, tilting of the molecular axis, and screening of the electric field by dipole-dipole coupling, so coverages cannot be readily inferred from the IR signal.[67-69] Considering these factors, and the relatively poor signal-to-noise ratio in these data, we cannot rule out the presence of other, perhaps broad peaks, but the data are consistent with at least half, and possibly nearly all the CO molecules being in atop sites at all Ni coverages for which we were able to measure IR spectra. This is quite different from the behavior of CO on close-packed single crystal surfaces, where intermolecular repulsions prevent the occupation of nearest-neighbor atop sites, and high-coverage phases involve substantial occupation of bridge and/or three-fold sites.[44-46,48,49]

IV. DISCUSSION

A simplified model of the growth of Ni islands on Au(111) assumes second layer Ni forms in a commensurate layer on an incomplete first layer of Ni starting around a Ni coverage of $\sim 0.3\ ML$. We found this growth model to be consistent with surface resistivity measurements that showed essentially no additional surface resistivity due to Ni deposited in the coverage range where second layer Ni is expected to form.[26] In the same coverage range, however, the saturation

This manuscript was accepted by J. Chem. Phys. Click here to see the version of record.

CO coverage increases sharply, suggesting either that this growth model is incomplete, or that the surface chemistry of the islands is anomalous, allowing a much higher CO to surface Ni ratio than is seen on flat Ni surfaces. If second layer Ni simply covers first layer Ni, one would instead expect the saturation CO coverage to level off to a near constant value. In this high Ni coverage regime, we find a CO to surface Ni ratio close to one, along with the emergence of adsorption sites with higher binding energies, and primarily atop bonding observed with FTIR.

To account for this behavior, we propose a layer dependent adsorption model in which the Ni atoms in the first and second layers have different numbers of Au nearest neighbors and surface roughness. In the first layer, the data are consistent with the presence of Au nearest neighbors, affecting the Ni-CO bond. Previous experimental and theoretical studies have found the presence of Au nearest neighbors to Ni can weaken the Ni-CO bond, due primarily to ligand effects,[11, 19, 57, 58] and lead to preferential atop binding.[10] For first-layer Ni atoms, these neighbors could be the underlying Au atoms in the substrate. There is also evidence from STM images of intermixing of Au in the single-layer Ni islands,[30] even though the solubility of Au in bulk Ni is very low,[70] which could further enhance the ligand effect. During first layer island growth, CO coverages on the Ni are ~ 0.5 CO/Ni similar to saturation coverages of CO on a variety of pure Ni surfaces at similar temperatures as our experiments, including the (111) face, which is perhaps most relevant due to the Au(111) substrate.[37, 38, 44, 48, 54, 55] Studies of CO adsorption to Ni-Au alloys did not find surface Au concentrations to decrease the amount of CO adsorbed to available Ni, but only weakened the Ni-CO bond.[11, 12] In Cullen et al.'s STM study of Ni islands on Au(111), they found intermixed Au at all temperatures studied, with the concentration of Au in the islands increasing for annealing temperatures greater than 400 K, above our experimental

This manuscript was accepted by J. Chem. Phys. Click here to see the version of record.

temperatures.[30] The effects of intermixed Au in the islands could be explored by performing adsorption experiments at a range of annealing temperatures.

As the Ni coverage increases and island growth transitions to predominantly second layer, our TPD curves broaden towards higher temperatures, approaching the desorption temperature for atop CO on Ni(100), suggesting the emergence of new adsorption configurations with higher binding energies. Studies of CO adsorption to step and kink sites on Pt have found higher desorption temperatures and IR peak frequencies than CO on flat Pt,[71-77] and it is possible the large lattice mismatch between Ni and Au leads to surface roughness and the presence of step and kink or similar low-coordination sites. This high energy broadening in the TPD data could also be explained by a reduction in the number of neighboring Au atoms weakening the Ni-CO bond. Such a reduction is to be expected since the second-layer Ni atoms are not in direct contact with the Au substrate, and, if intermixing is a factor, it is possible that any diffusion of gold atoms into the second layer in the islands is less kinetically favorable at the relatively low temperatures used in this study. It is also possible the presence of CO alters the island composition in favor of higher Ni concentration, as gas conditions are known to influence alloy composition and surface structure.[12, 78] A study of Ni-Au clusters on TiO_2 found CO could induce diffusion of Ni to the surface of the clusters due to the strong Ni-CO bond.[12]

Yang et al. found Au's effect to lead to preferential binding of atop CO to Ni over a range of Au concentrations in Ni-Au alloys,[10] implying we would not necessarily expect IR absorption behavior to show much variation due to changes in Au concentration in the islands.

Perhaps the most striking observation in this work is the shift during second layer island growth of the CO to surface Ni atom ratio from ~ 0.5 CO/Ni towards ~ 1 CO/Ni. These high saturated CO coverages at the highest Ni coverages on Au(111) in Figure 5, are significantly

This manuscript was accepted by J. Chem. Phys. Click here to see the version of record.

higher than typical saturated CO coverages on extended Ni surfaces of 0.5 - 0.67 ML.[37, 44, 48, 54, 55] Even more surprising, we measure CO only in the atop site, while saturated CO on extended surfaces also occupies two- and three-fold adsorption sites.[44] Because bridge CO tends to have broader and smaller IR peaks than atop CO, it is certainly possible that on these islands there is undetected bridge CO, hidden in the noise of our FTIR signals. However, there is sufficient intensity in the atop signal to account for most if not all of the adsorbed CO. Huang et al. found the bond weakening effect of Au on the Ni-CO bond was site dependent, with the largest effect for bridge CO.[19] Due to the number of Au nearest neighbors to the Ni atoms, bridge CO may no longer be energetically possible at the temperatures in this experiment, but experiments done at lower temperatures might measure bridge CO.

As mentioned, the higher binding energy adsorption sites seen during second layer growth are consistent with both a reduction in the number of Au nearest neighbors to Ni atoms and the presence of step and edge sites. The STM images of Hannemann et al. show spiral structures within the islands that could be due to internal strain.[22] We suggest these corrugated, and possibly expanded structures with intermixed Au, lead to preferential atop binding and allow CO molecules to bind at larger nearest neighbor distances than on extended surfaces. Larger nearest neighbor distances could reduce steric repulsion, and allow for the higher CO coverages we observe. The three-dimensional structure of the islands could also accommodate out-of-plane tilting of some of the CO, further reducing steric interactions and partially accounting for the relative constancy of the IR intensity as CO coverage increases.

Given the heterogeneous structure of the Ni islands, we would expect the presence of diverse CO binding environments to result in significant inhomogeneous broadening of the C=O vibration. It is surprising, then, that we observe linewidths (FWHM) of $16 - 35\ cm^{-1}$ (with

This manuscript was accepted by J. Chem. Phys. Click here to see the version of record.

16 cm^{-1} instrumental resolution, so the lowest value is an upper limit on the true linewidth), compared to $\sim 35\ cm^{-1}$ on Ni(100) in our system (8 cm^{-1} resolution), and $25 - 40\ cm^{-1}$ measured by Lauterbach et al. on Ni(100).[37] We suggest that these narrow linewidths at saturation coverage are due to strong dipole coupling, which tends to concentrate the IR absorption signal into a single narrow coherent mode.[67, 68, 79] Since the strength of the coupling varies as the inverse cube of the intermolecular distance,[38] we would expect very strong coupling at the anomalously high local CO densities observed on the islands.

Strong dipole coupling could also account for the upward shift in ν_{peak} seen in Fig. 6.[79] Generally frequency shifts arise from a combination of chemical and dipole effects. As CO packing density increases, chemical effects might be expected to decrease ν_{peak} via the Blyholder mechanism,[56] but the observed overall upward shift suggests that the upward dipole shift dominates. Experiments using different isotopes of CO could determine the presence and relative magnitudes of these effects.

In addition to the TPD and FTIR measurements made in this experiment, we also monitored the surface resistivity ρ_s, of the Au(111) sample during both Ni island growth and CO exposure. Adsorbate induced changes to ρ_s are due to the scattering of conduction electrons by the adsorbates, and studies have found that only adsorbates in direct contact with the substrate produce a measurable effect on ρ_s.[31-34] CO has a significantly higher scattering cross section than Ni,[80] so it is reasonable that CO adsorbed to first layer Ni could cause a measurable change to ρ_s, even though no such change was observed for second-layer Ni.

Figure 8 shows typical data for surface resistivity during CO exposure (5L), where the shaded region indicates CO exposure. We measured no change in resistance due to CO adsorption, indicating any changes to resistance are < 0.02%, consistent with no CO being in direct contact with the Au substrate, and indicating, consistent with our observations for second-layer Ni deposition,[26] that Au conduction electrons do not penetrate into the island and scatter. For comparison, the inset of Figure 8 shows ~ 0.5% surface resistivity change due to first layer Ni growth on the Au.[26]

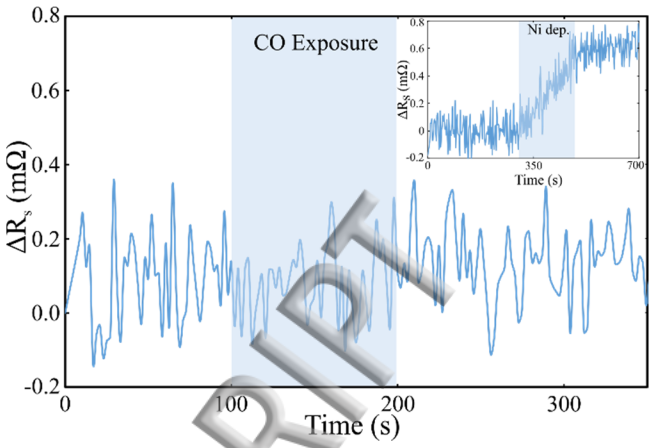

Figure 8: Measured resistance trace during CO exposure on Ni/Au(111) as a function of time. CO Exposure begins around 100 s and ends around 200 s, as indicated by the shaded region. We find no measurable changes in resistivity due to CO adsorption. For comparison, inset shows measured resistance change during first layer Ni growth, where the shaded region indicates Ni deposition. At $t = 0$, $R_s \approx 100\ m\Omega/sq$.

V. CONCLUSIONS

We observe a large increase in saturation CO adsorption to Ni nanoislands as the islands begin to grow a second layer. Local CO coverage on the Ni rises from ~ 0.5 CO/Ni towards ~ 1 CO/Ni in the region of second Ni layer growth. The type of adsorption seen in this system is quite different than CO adsorption on flat, extended Ni surfaces, underscoring the novel and complex surface chemistry that can arise in nanoscale particles. Our observations share some characteristics of bimetallic and highly stepped adsorption systems.[10, 11, 17] We propose a layer-dependent adsorption model where the number of Au nearest neighbors and amount of surface roughness strongly influence the Ni-CO adsorption properties. During first layer island growth,

the Au substrate and possible presence of intermixed Au in the islands leads to a decrease in peak desorption temperatures compared to pure Ni, and a preference for atop sites. As the second island layer grows, the surface Ni atoms have fewer Au nearest neighbors, and surface roughness increases, leading to a CO coverage approaching 1 CO/Ni, occupation of sites with higher binding energy, and still only atop CO. Additional experiments that control Au surface concentrations through annealing could help clarify and separate the effects of chemical environment, surface structure, and surface strain.

VI. ACKNOWLEDGEMENTS

JIC gratefully acknowledges support from a John F. Burlingame Fellowship from Tufts University. The authors thank the Tufts Faculty Research Awards Committee for partial support of this research. We also thank Jordan Kemp and Natalie Bohm for technical assistance.

REFERENCES

[1] V. H. Grassian, Journal of Physical Chemistry C **112** (2008) 18303.

[2] H. Z. Zhang, R. L. Penn, R. J. Hamers, and J. F. Banfield, J. Phys. Chem. B **103** (1999) 4656.

[3] H. M. Lu, Z. Wen, and Q. Jiang, Chemical Physics **309** (2005) 303.

[4] K. Furusawa, Z. Shou, and N. Nagahashi, Colloid and Polymer Science **270** (1992) 212.

[5] J. E. B. Katari, V. L. Colvin, and A. P. Alivisatos, Journal of Physical Chemistry **98** (1994) 4109.

[6] I. Luzinov, I. Evchuk, S. Minko, and S. Voronov, Journal of Applied Polymer Science **67** (1998) 299.

[7] W. T. Wallace, and R. L. Whetten, J. Phys. Chem. B **104** (2000) 10964.

[8] R. Lazzari, J. Goniakowski, G. Cabailh, R. Cavallotti, N. Trcera, P. Lagarde, and J. Jupille, Nano Letters **16** (2016) 2574.

[9] S. E. Bae, D. Gokcen, P. Liu, P. Mohammadi, and S. R. Brankovic, Electrocatalysis **3** (2012) 203.

[10] F. Yang, Y. X. Yao, Z. Yan, H. Min, and D. W. Goodman, Applied Surface Science **283** (2013) 263.

[11] P. M. Holmblad, J. H. Larsen, and I. Chorkendorff, Journal of Chemical Physics **104** (1996) 7289.

[12] S. A. Tenney, W. He, C. C. Roberts, J. S. Ratliff, S. I. Shah, G. S. Shafai, V. Turkowski, T. S. Rahman, and D. A. Chen, Journal of Physical Chemistry C **115** (2011) 11112.

[13] Z.-T. Wang, M. T. Darby, A. J. Therrien, M. El-Soda, A. Michaelides, M. Stamatakis, and E. C. H. Sykes, The Journal of Physical Chemistry C **120** (2016) 13574.

[14] M. Ruff, N. Takehiro, P. Liu, J. K. Norskov, and R. J. Behm, Chemphyschem **8** (2007) 2068.

[15] F. Gao, and D. W. Goodman, Chemical Society Reviews **41** (2012) 8009.

[16] A. Schlapka, M. Lischka, A. Gross, U. Kasberger, and P. Jakob, Physical Review Letters **91**, 016101 (2003)

[17] B. Hammer, O. H. Nielsen, and J. K. Norskov, Catalysis Letters **46** (1997) 31.

[18] J. R. Kitchin, J. K. Norskov, M. A. Barteau, and J. G. Chen, Physical Review Letters **93**, 156801 (2004)

[19] Y. C. Huang, J. Y. Du, T. Zhou, and S. F. Wang, Chemphyschem **13** (2012) 3909.

[20] M. Mavrikakis, B. Hammer, and J. K. Norskov, Physical Review Letters **81** (1998) 2819.

[21] A. J. Therrien, A. Pronschinske, C. J. Murphy, E. A. Lewis, M. L. Liriano, M. D. Marcinkowski, and E. C. H. Sykes, Physical Review B **92**, 161407 (2015)

[22] H. Hannemann, C. A. Ventrice, T. Bertrams, A. Brodde, and H. Neddermeyer, Physica Status Solidi a-Applied Research **146** (1994) 289.

[23] C. A. Ventrice, T. Bertrams, H. Hannemann, A. Brodde, and H. Neddermeyer, Physical Review B **49** (1994) 5773.

[24] J. A. Meyer, I. D. Baikie, E. Kopatzki, and R. J. Behm, Surface Science **365** (1996) L647.

[25] A. G. Trant, T. E. Jones, J. Gustafson, T. C. Q. Noakes, P. Bailey, and C. J. Baddeley, Surface Science **603** (2009) 571.

[26] J. I. Cohen, and R. G. Tobin, Journal of Chemical Physics **146**, 144703 (2017) 7.

[27] D. D. Chambliss, R. J. Wilson, and S. Chiang, Physical Review Letters **66** (1991) 1721.

[28] D. D. Chambliss, R. J. Wilson, and S. Chiang, Journal of Vacuum Science & Technology B **9** (1991) 933.

[29] W. Chen, V. Madhavan, T. Jamneala, and M. F. Crommie, Physical Review Letters **80** (1998) 1469.

[30] W. G. Cullen, and P. N. First, Surface Science **420** (1999) 53.

[31] C. Liu, and R. G. Tobin, Journal of Chemical Physics **128**, 244702 (2008)

[32] C. Liu, and R. G. Tobin, Journal of Chemical Physics **126**, 124705 (2007)

[33] C. L. Hsu, E. F. McCullen, and R. G. Tobin, Surface Science **542** (2003) 120.

[34] H. Grabhorn, A. Otto, D. Schumacher, and B. N. J. Persson, Surface Science **264** (1992) 327.

[35] N. Hayashi, and K. Kawasaki, Journal of Catalysis **48** (1977) 243.

[36] P. Wissmann, and K.Muller, Springer Tracts in Modern Physics 77 (1975)

[37] J. Lauterbach, M. Wittmann, and J. Kuppers, Surface Science **279** (1992) 287.

[38] J. C. Campuzano, and R. G. Greenler, Surface Science **83** (1979) 301.

[39] R. G. Tobin, S. Chiang, P. A. Thiel, and P. L. Richards, Surface Science **140** (1984) 393.

[40] S. Andersson, Solid State Communications **21** (1977) 75.

[41] R. Klauser, W. Spiess, A. M. Bradshaw, and B. E. Hayden, Journal of Electron Spectroscopy and Related Phenomena **38** (1986) 187.

[42] A. Grossmann, W. Erley, and H. Ibach, Surface Science **366** (1996) L742.

[43] J. C. Bertolini, and B. Tardy, Surface Science **102** (1981) 131.

[44] V. Shah, T. Li, K. L. Baumert, H. S. Cheng, and D. S. Sholl, Surface Science **537** (2003) 217.

[45] K. Christmann, O. Schober, and G. Ertl, Journal of Chemical Physics **60** (1974) 4719.

[46] D. C. Skelton, D. H. Wei, and S. D. Kevan, Surface Science **370** (1997) 64.

[47] P. T. Sprunger, F. Besenbacher, and I. Stensgaard, Chemical Physics Letters **243** (1995) 439.

[48] M. Trenary, K. J. Uram, and J. T. Yates, Surface Science **157** (1985) 512.

[49] G. C. Bond, C. Louis, and D. T. Thompson, *Catalysis by Gold* 2006), Vol. 6, Catalysis by Gold,

[50] P. Dumas, R. G. Tobin, and P. L. Richards, Surface Science **171** (1986) 555.

[51] C. Ruggiero, and P. Hollins, Journal of the Chemical Society-Faraday Transactions **92** (1996) 4829.

[52] A. M. Bradshaw, and J. Pritchard, Proceedings of the Royal Society of London Series a-Mathematical and Physical Sciences **316** (1970) 169.

[53] D. A. Outka, and R. J. Madix, Surface Science **179** (1987) 351.

[54] L. Surnev, Z. Xu, and J. T. Yates, Surface Science **201** (1988) 1.

[55] G. Held, J. Schuler, V. Sklarek, and H. P. Steinruck, Surface Science **398** (1998) 154.

[56] G. Blyholder, Journal of Physical Chemistry **68** (1964) 2772.

[57] K. Termentzidis, and J. Hafner, Journal of Physics-Condensed Matter **19**, 246219 (2007)

[58] K. Termentzidis, J. Hafner, and F. Mittendorfer, Journal of Physics-Condensed Matter **18** (2006) 10825.

[59] Samples purchased from Structure Probe, Inc. Item Number 466PS-AB

[60] E. T. Krastev, and R. G. Tobin, Journal of Vacuum Science & Technology a-Vacuum Surfaces and Films **16** (1998) 743.

[61] Silver Print II from GC Electronics Part No. 22-023

[62] N. Takeuchi, C. T. Chan, and K. M. Ho, Physical Review B **43** (1991) 13899.

[63] G. E. Becker, and H. D. Hagstrum, Journal of Vacuum Science & Technology **11** (1974) 284.

[64] P. A. Redhead, Vacuum **12** (1962) 203.

[65] D. M. Collins, and W. E. Spicer, Surface Science **69** (1977) 85.

[66] G. A. Somorjai, Surface Science **242** (1991) 481.

[67] R. Ryberg, Surface Science **114** (1982) 627.

[68] B. N. J. Persson, and R. Ryberg, Physical Review B **24** (1981) 6954.

[69] R. G. Greenler, Journal of Chemical Physics **44** (1966) 310.

[70] P. Franke, and D. Neuschütz, in *Binary Systems. Part 5: Binary Systems Supplement 1: Phase Diagrams, Phase Transition Data, Integral and Partial Quantities of Alloys*, edited by P. Franke, and D. Neuschütz (Springer Berlin Heidelberg, Berlin, Heidelberg, 2007), pp. 1.

[71] H. Froitzheim, H. Hopster, H. Ibach, and S. Lehwald, Applied Physics **13** (1977) 147.

[72] A. Garnier, S. Sall, F. Garin, M. J. Chetcuti, and C. Petit, J. Mol. Catal. A-Chem. **373** (2013) 127.

[73] R. J. Mukerji, A. S. Bolina, and W. A. Brown, Surface Science **527** (2003) 198.

[74] M. J. Lundwall, S. M. McClure, and D. W. Goodman, Journal of Physical Chemistry C **114** (2010) 7904.

[75] J. S. Luo, R. G. Tobin, D. K. Lambert, G. B. Fisher, and C. L. Dimaggio, Surface Science **274** (1992) 53.

[76] B. E. Hayden, K. Kretzschmar, A. M. Bradshaw, and R. G. Greenler, Surface Science **149** (1985) 394.

[77] S. C. Creighan, R. J. Mukerji, A. S. Bolina, D. W. Lewis, and W. A. Brown, Catalysis Letters **88** (2003) 39.

[78] D. C. Skelton, R. G. Tobin, D. K. Lambert, C. L. DiMaggio, and G. B. Fisher, Sensors and Actuators B-Chemical **96** (2003) 46.

[79] B. N. J. Persson, and R. Ryberg, Chemical Physics Letters **174** (1990) 443.

[80] B. N. J. Persson, Journal of Chemical Physics **98** (1993) 1659.

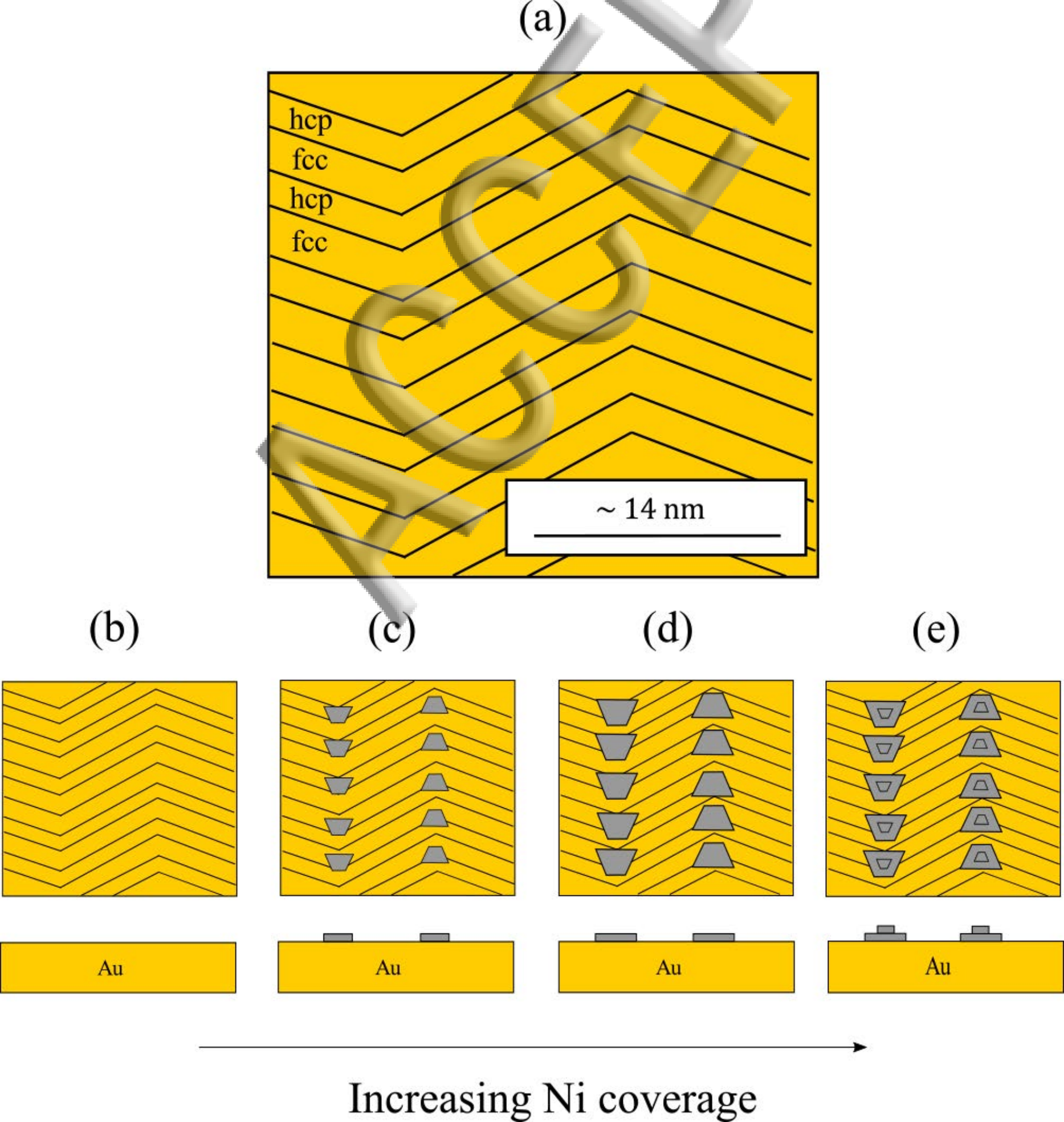
(a)
hcp
fcc
hcp
fcc
~ 14 nm
(b)
(c)
(d)
(e)
Au
Au
Au
Au
Increasing Ni coverage

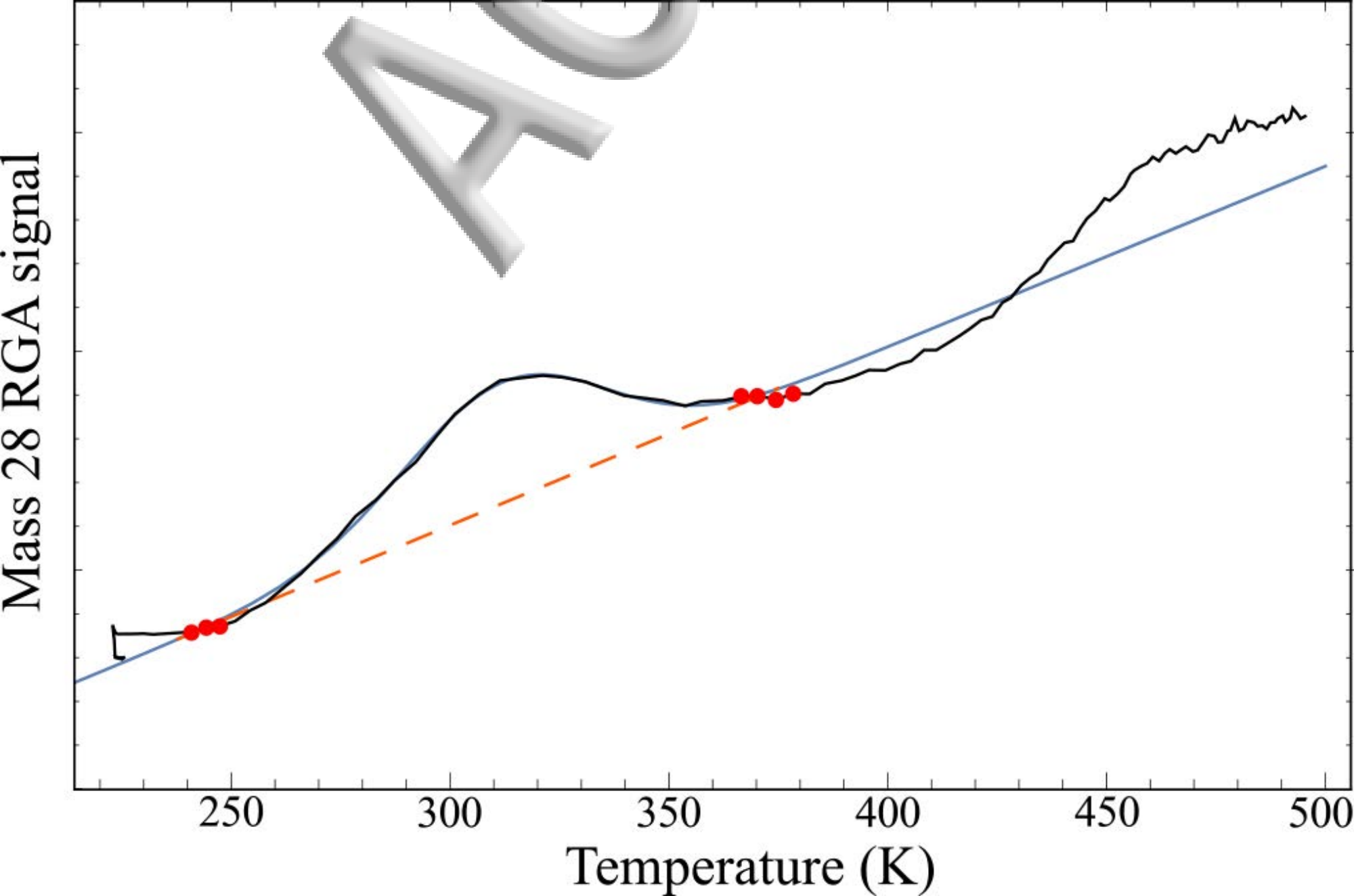
Mass 28 RGA signal
250
300
350
400
450
500
Temperature (K)

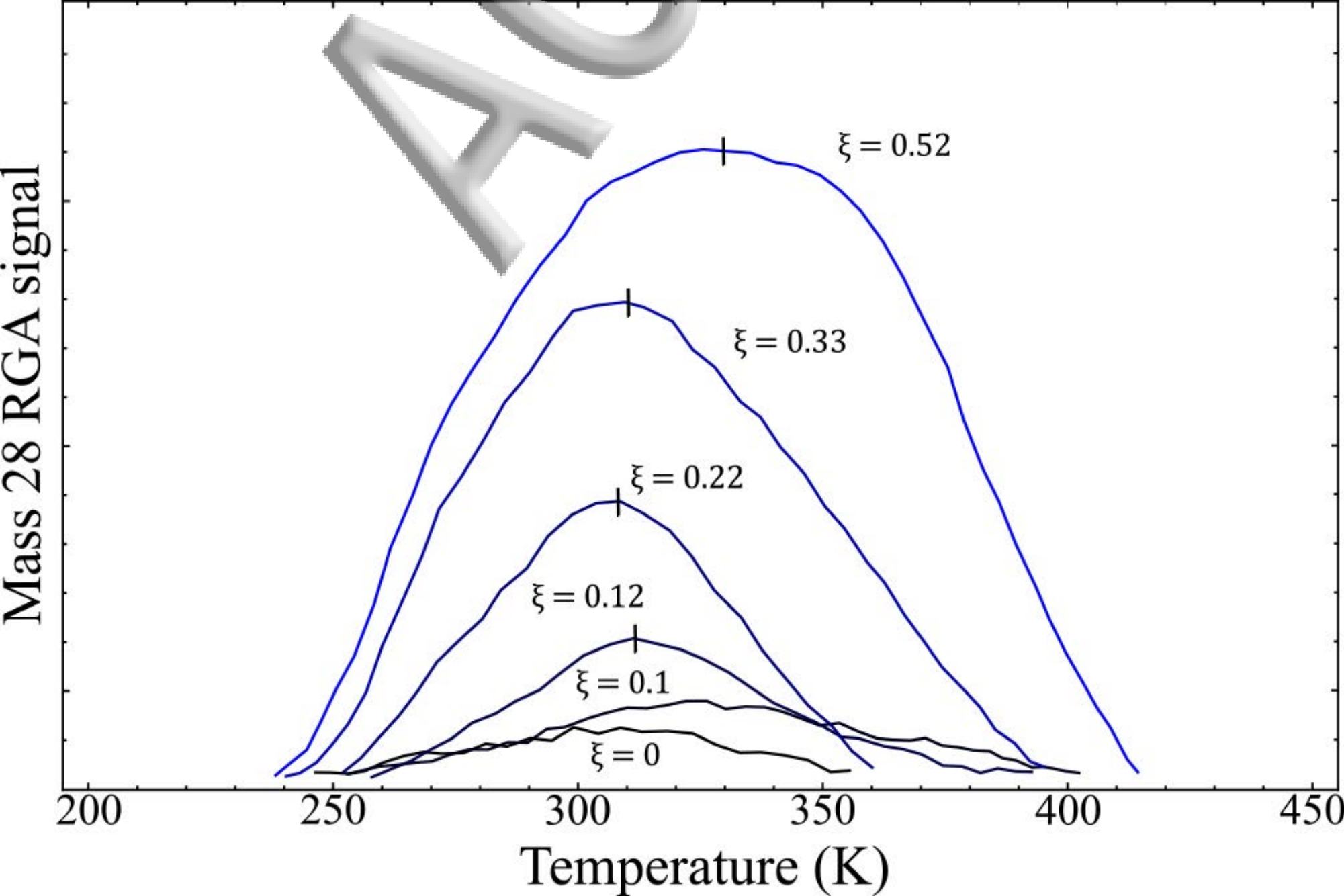
ξ = 0.52
ξ = 0.33
ξ = 0.22
ξ = 0.12
ξ = 0.1
ξ = 0
Mass 28 RGA signal
200
250
300
350
400
450
Temperature (K)

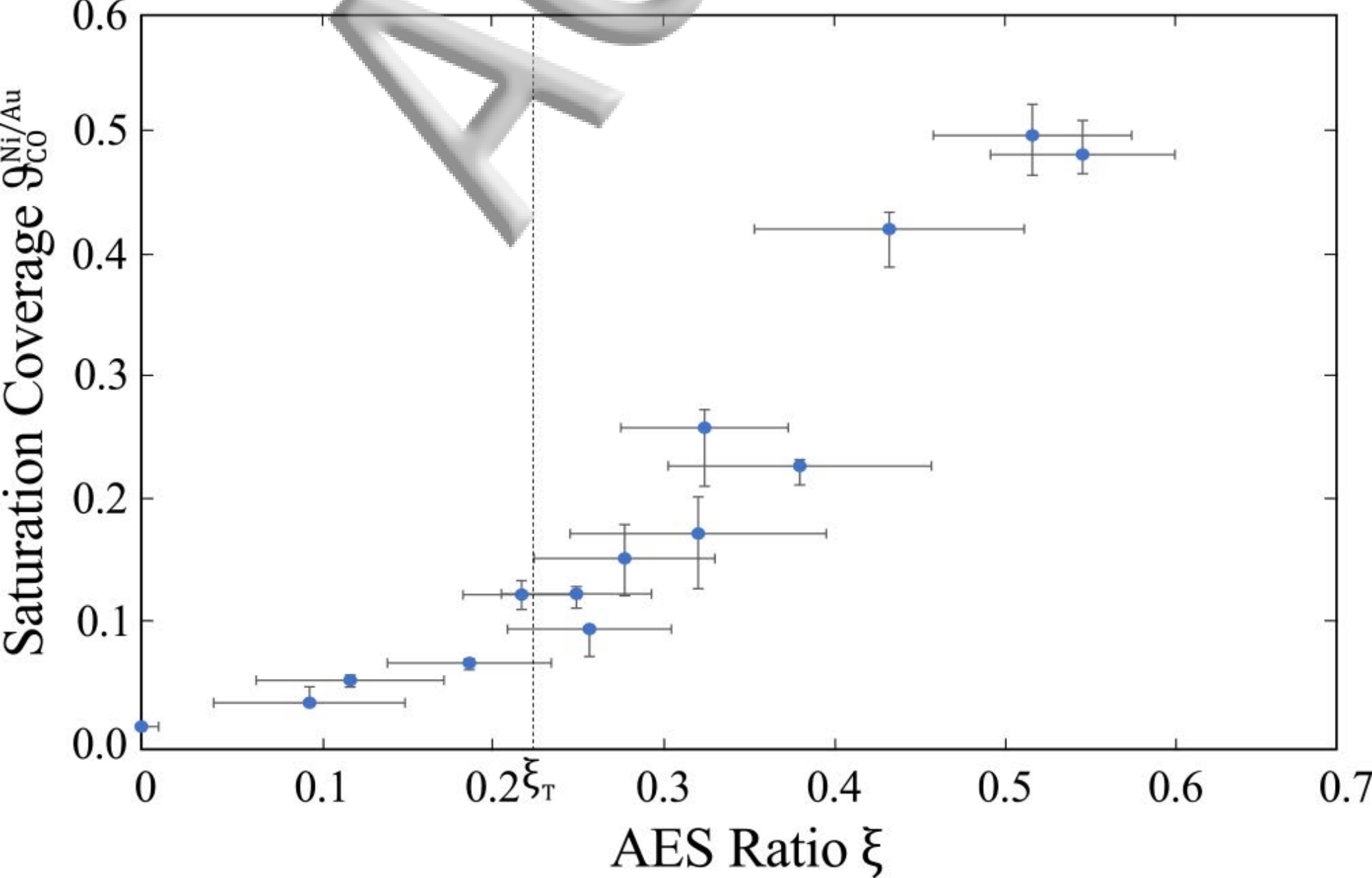
Saturation Coverage $\vartheta_{CO}^{Ni/Au}$
AES Ratio ξ
0.0
0.1
0.2
0.3
0.4
0.5
0.6
0
0.1
0.2
ξT
0.3
0.4
0.5
0.6
0.7

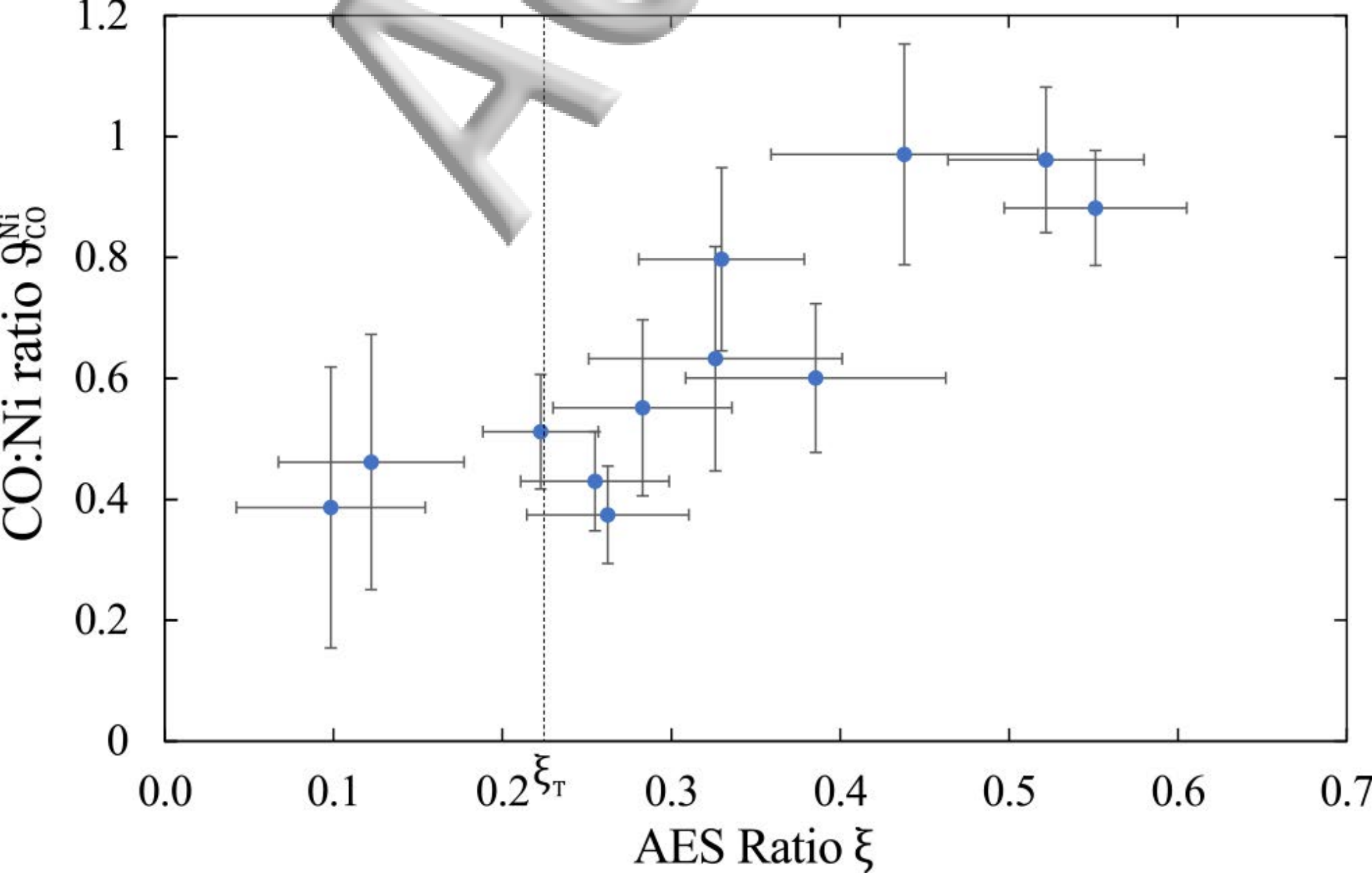
CO:Ni ratio ϑ_{CO}^{Ni}
AES Ratio ξ
ξ_T
0
0.2
0.4
0.6
0.8
1
1.2
0.0
0.1
0.2
0.3
0.4
0.5
0.6
0.7

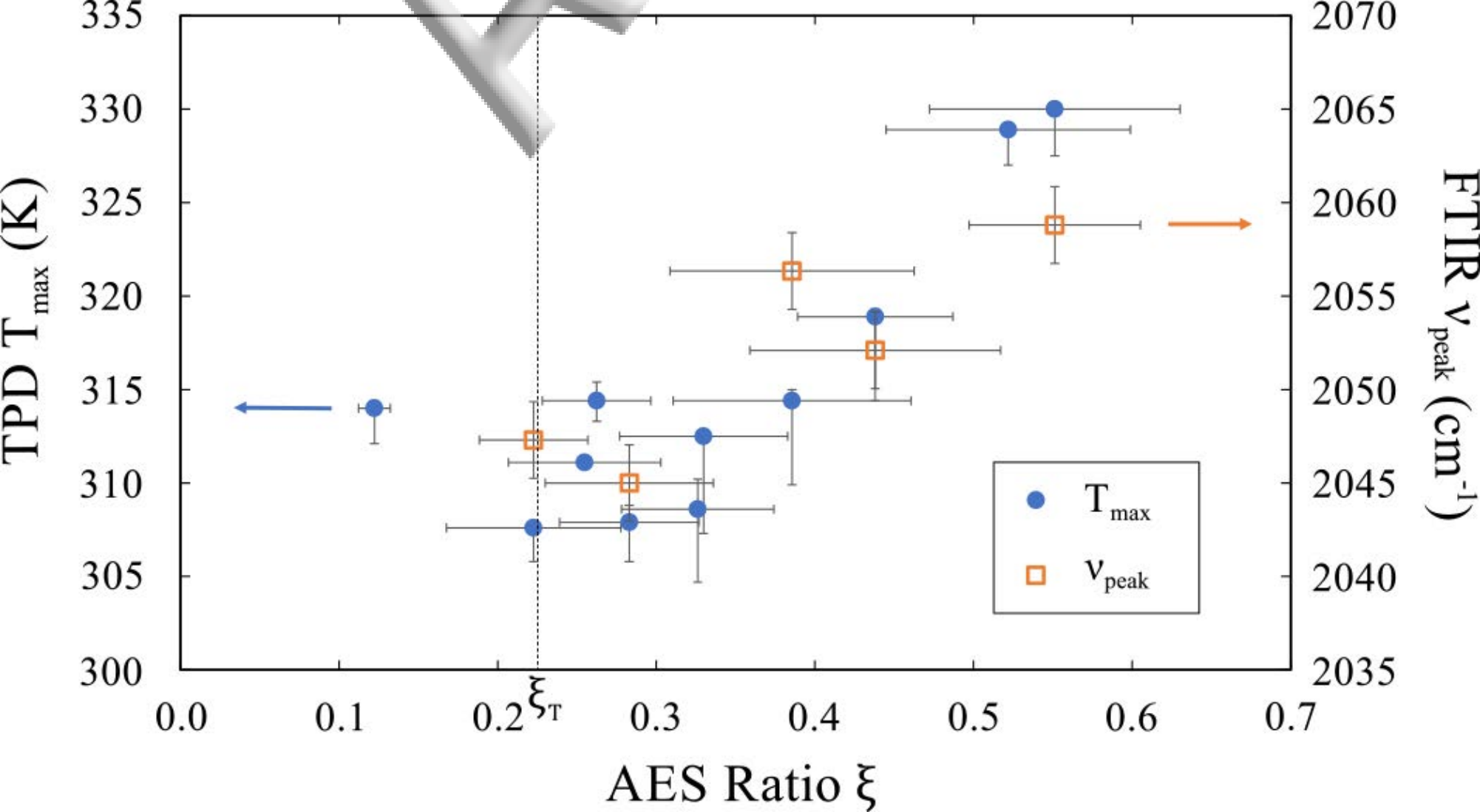
TPD T_{max} (K)
FTIR ν_{peak} (cm^{-1})
AES Ratio ξ
ξ_T
T_{max}
ν_{peak}
335
330
325
320
315
310
305
300
2070
2065
2060
2055
2050
2045
2040
2035
0.0
0.1
0.2
0.3
0.4
0.5
0.6
0.7

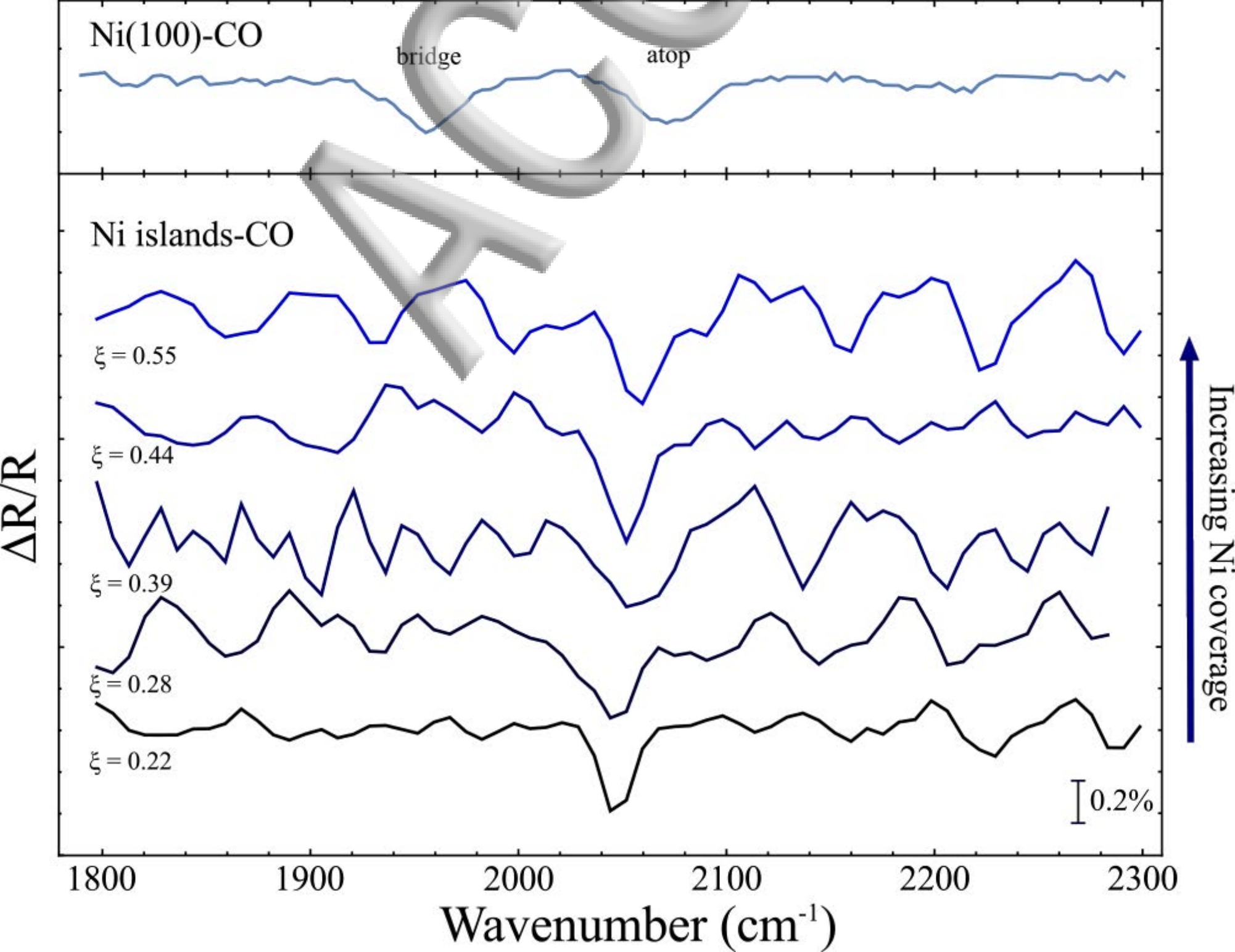
Ni(100)-CO
bridge
atop
Ni islands-CO
ξ = 0.55
ξ = 0.44
ξ = 0.39
ξ = 0.28
ξ = 0.22
0.2%
ΔR/R
Increasing Ni coverage
1800
1900
2000
2100
2200
2300
Wavenumber (cm-1)

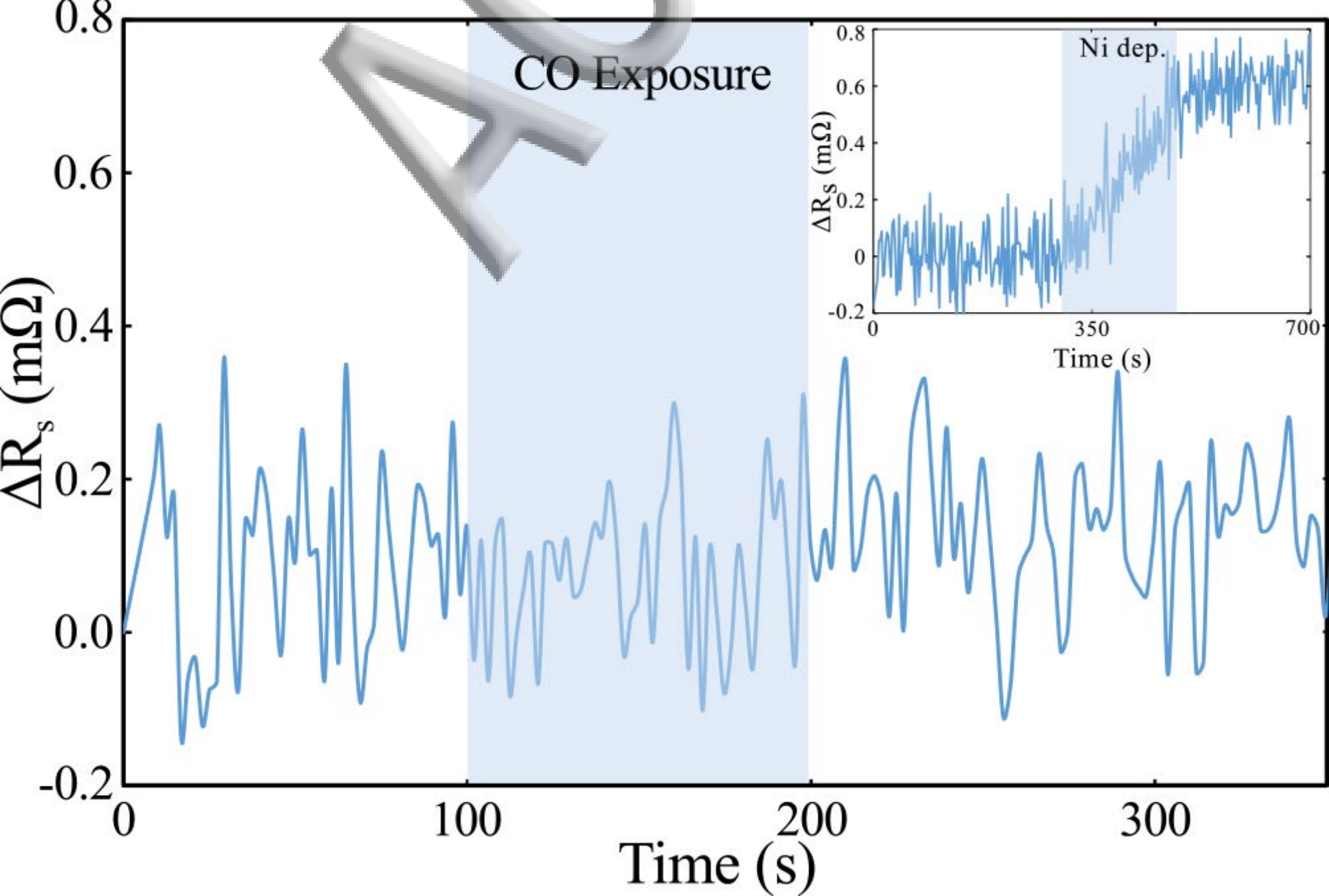
CO Exposure
Ni dep.
ΔRs (mΩ)
Time (s)
0.8
0.6
0.4
0.2
0.0
-0.2
0
100
200
300
350
700